Bioaeroelastic linear stability analysis and nonlinear time simulations

Résumé du chapitre 4

Le premier objectif de ce chapitre est d'illustrer comment les modèles de véhicule et de pilote développés dans les deux chapitres précédents peuvent être assemblés afin d'obtenir le comportement bio-aéroélastique du système global. Il est notamment montré, par comparaison entre l'espace Cartésien, voir Figure 4-1, et « l'espace » des bond graphs, voir Figure 4-2, comment ces deux espaces partagent des frontières communes explicites, faisant du bond graph une approche de modélisation dite « structurelle ».
Dans un deuxième temps, une analyse linéaire de la stabilité est menée sur les axes latéral et de roulis d'un modèle bio-aéroélastique d'hélicoptère en vol stationnaire. Cette analyse révèle que les modes qui peuvent potentiellement être déstabilisés sont les modes dits de « traînées » de rotors articulés. La déstabilisation du mode régressif de « trainée » par le comportement biodynamique est conjecturée dans (Muscarello, et al., 2015)*. Le modèle présenté ici appui cette conclusion, voir Figure 4-5. De plus, l'analyse révèle que le mode progressif de « traînée » peut également être déstabilisé par le pilote ; une expérience est néanmoins nécessaire afin de confirmer ou d'infirmer cette analyse. En parallèle, des résultats de simulations dans le domaine temporel, obtenus à partir du modèle bio-aéroélastique non linéaire en bond graphs, sous 20-sim ®, de la réponse libre du système sont présentés, voir Figure 4-7. Dans les cas choisis, on peut observer que selon l'état neuromusculaire du pilote, celui-ci peut participer à la déstabilisation de l'hélicoptère à des fréquences au voisinage de $\Omega-\omega_\delta$ ($\approx$ 3 Hz) ou $\Omega+\omega_\delta$ ($\approx$ 7 Hz). Il faut toutefois tempérer les conclusions en tenant compte des hypothèses fortes qui ont été faites, notamment en ce qui concerne le modèle aérodynamique qui n'est que quasi-statique et le modèle de comportement de pilote qui est approximé au comportement d'un système du second-ordre. Dans tous les cas, des résultats d'essais en vol semblent nécessaires pour pouvoir avancer.*

The first objective of this chapter is to describe how the vehicle and pilot bond graph models developed in the previous chapters can be assembled to represent the bioaeroelastic behavior of the global system. Secondly, a linear stability analysis on the lateral-roll axis of a helicopter is performed, revealing the modes that can be eventually destabilized; finally time simulations are performed from the nonlinear model and seem to be in agreement with the linear model conclusions and give an appreciation of what could be observed in the Cartesian space when this phenomenon occurs.

4.1. Pilot-vehicle system bond graph

4.1.1. Bond graphs for a structural modeling approach

From the bond graph models of both helicopter and pilot developed in the previous chapters, one can assemble them into one graph as illustrated on Figure 4-2. In the Cartesian space this is equivalent to what can be seen on Figure 4-1, where the point P_1 is the center of the spherical joint between the pilot's arm and the cockpit of the helicopter. The points P_2 to P_9 are attachment points of muscles between the pilot and the cockpit. The implicit assumption made here is that the pilot's torso cannot move in the seat and the seat cannot move either with respect to the cockpit.
Interestingly, one can see the points that appear in the physical space are materialized at the bond graph level see Figure 4-1 and Figure 4-2. The frontiers of the system's subsystems are explicitly represented, and the physical quantity that is exchanged between them is power. This is why the bond graph method is said to be *structural* (Chikhaoui, 2013)*;* in other words, the global bond graph of a complex system can be decomposed into sub graphs that have the same frontiers as the physical subsystems.

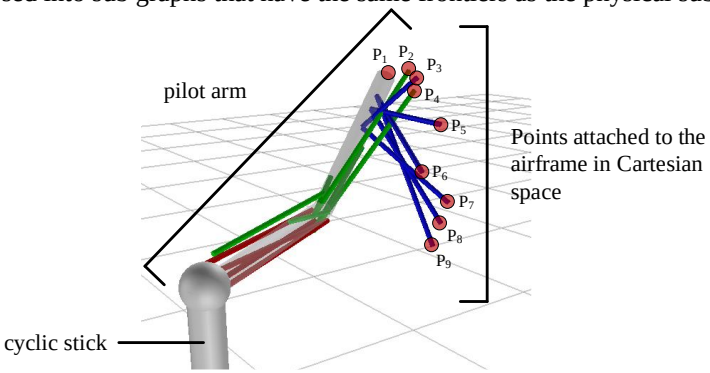

Figure 4-1. Attachment points of the pilot arm model on the airframe

The power exchanged between the pilot arm and the helicopter airframe through the point P_1 is the result of the product of both static and kinematic screws[16],

[16] *Torseur* in French

$$P_{P_1} = \mathbf{F}_{0\to arm}.\mathbf{V}_{P_1,arm/0} + \mathbf{M}_{P_1,0/arm}.\boldsymbol{\Omega}_{arm/0} \tag{60}$$

The green and purple arrows behind P_1 on Figure 4-2 respectively transport the force-velocity and the angular velocity-moment products.
For the rest of the points P_i of Figure 4-1 for *i* between 2 and 9, the power exchanged expression is,

$$P_{P_i} = \mathbf{F}_{Muscle\ i\to airframe}.\mathbf{V}_{P_i,airframe/0} \tag{61}$$

This quantity is materialized on the graph Figure 4-2 by the green arrow behind each P_i point (for *i* between 2 and 9).

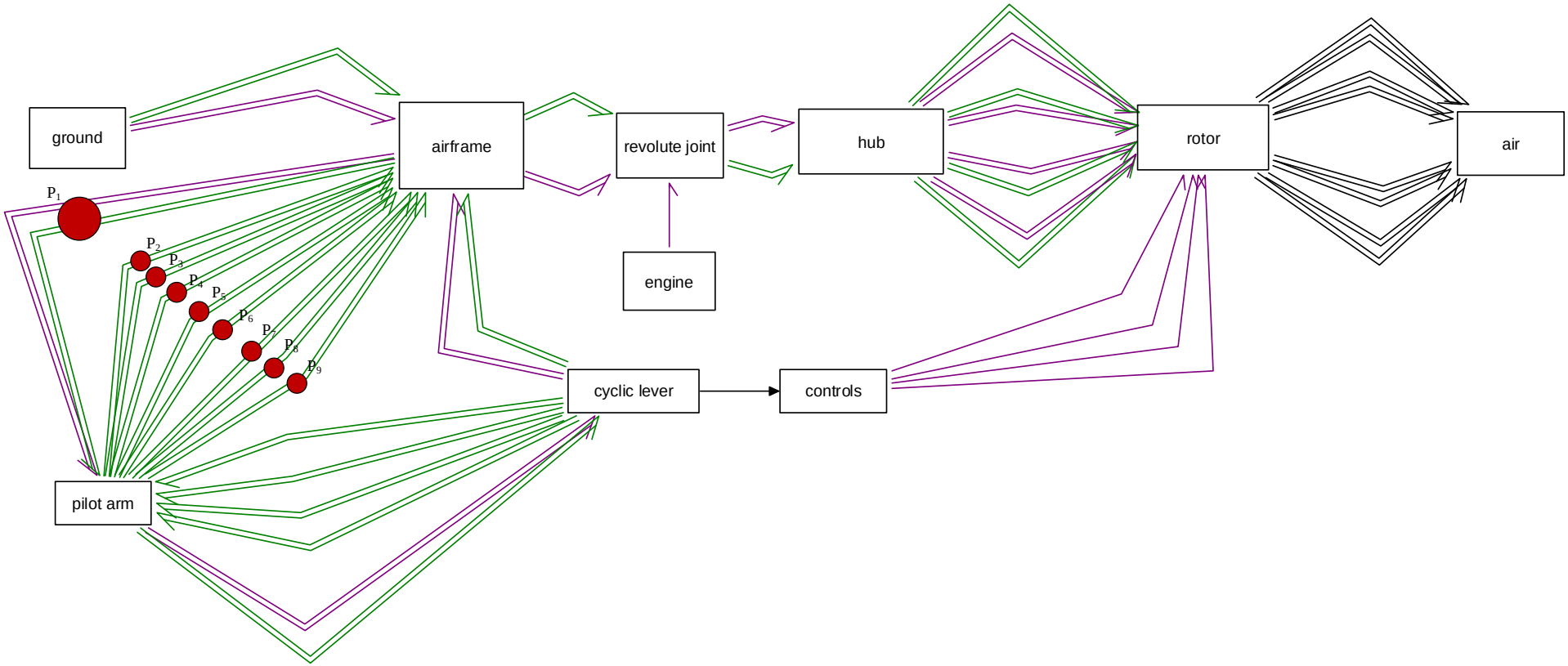

Figure 4-2. Rotorcraft bioaeroelastic system model using bond graphs

4.1.2. Pilot biodynamics model order reduction

The pilot biodynamics model developed in the previous chapter can be used in several manners. The first one consists in directly analyzing the resulting bioaeroelastic model developed previously for which several flight conditions and cabin configurations could be virtually simulated and explored. A second approach, consists in coupling a given vehicle model with a pilot model obtained by identification from experimental results or numerical simulation results, see Figure 4-4.
In order to see how the involuntary pilot behavior can affect the stability of a helicopter on its lateral-roll axis, it is proposed to use the second approach and to perform a sweep of potential pilot neuromuscular system's behaviors for a given helicopter. Furthermore, in order to be able to use powerful stability analysis tools such as Lyapunov's indirect method (eigenvalue analysis of dynamic system's state space matrix) and Campbell diagrams[17], the pilot model is proposed to be reduced to a second order model, as follows,

$$bdft(s) = \frac{\theta_{lat}}{\ddot{x}} \approx \frac{k.\omega^2}{\omega^2 + 2.\zeta.\omega.s + s^2} \tag{62}$$

It also allows reducing the computational cost and more importantly to give the possibility to sweep a wide range of potential involuntary pilot behaviors.

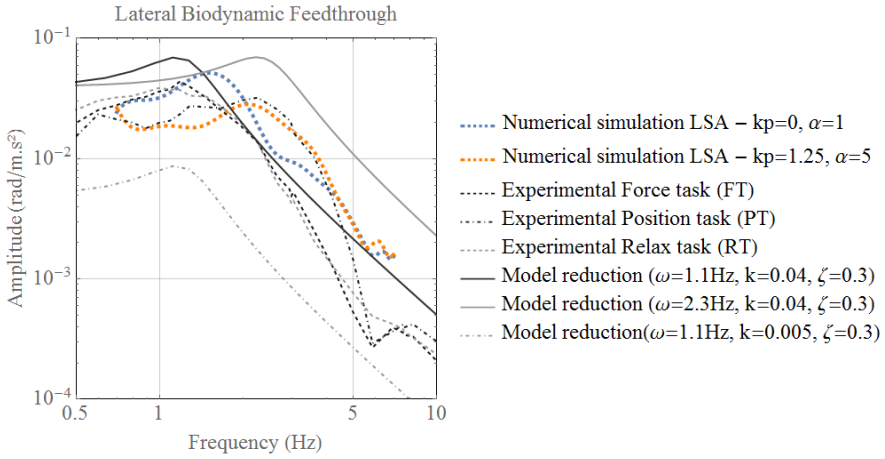

Figure 4-3. Biodynamic feedthrough envelop reduced models

[17] Campbell diagrams are especially used in the investigation of parametric instabilities that might occur in rotating systems. An application is given on Figure 4-6. A classic helicopter parametric instability known as ground resonance is detailed in the next chapter.

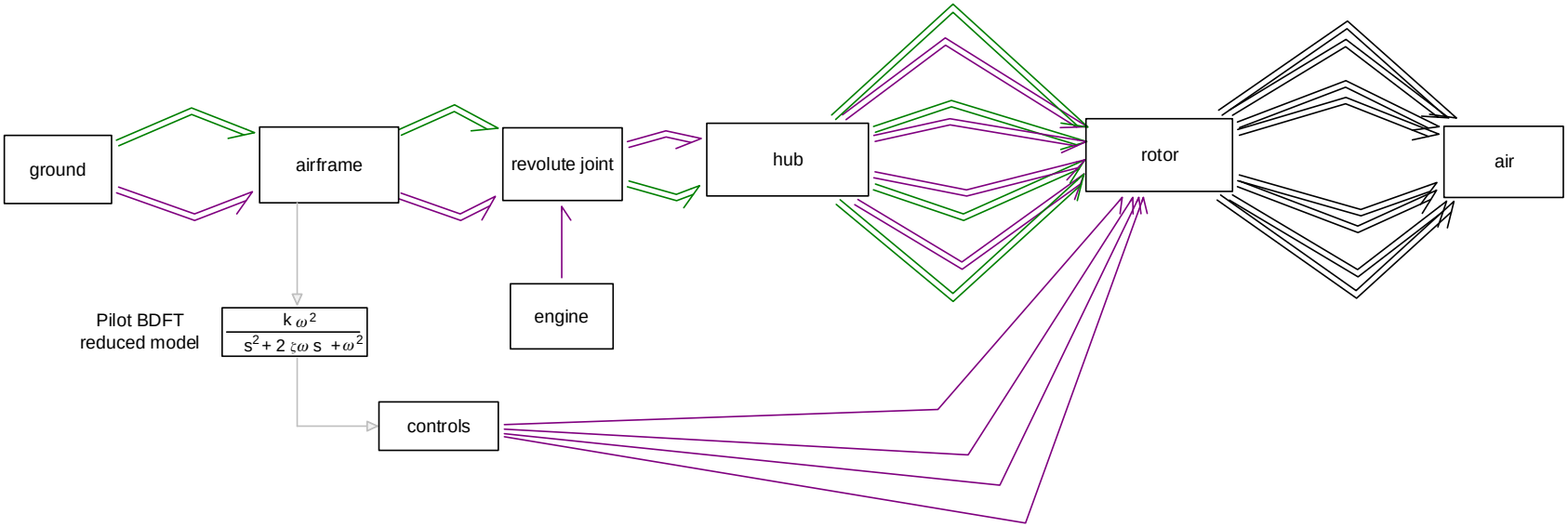

Figure 4-4. Bioaeroelastic system with a reduced BDFT pilot model

On Figure 4-3, the experimental results come from (Venrooij, et al., 2011) on the top of what, the numerical simulations results (LSA – least squares approximation) of the previous chapters have been superposed. The three model reductions presented on the same figure represent three different pilot neuromuscular model setups for which the gain *k* and the resonant frequency ω of the transfer function on equation (62) vary: the higher these parameters are, the 'stiffer' one could qualify the pilot involuntary behavior. These are the same quantities that are swept over a wide range of value on Figure 4-5.

4.2. Lateral-roll axis linear stability analysis and nonlinear time simulations

In this section, the models developed previously are analyzed, in particular on the lateral-roll axis of the helicopter. First a linear model is analyzed and then nonlinear time simulations are carried out.

4.2.1. Linear stability analysis results

The linearized equations from the vehicle model could have been obtained from the bond graph and would give the same results than the state space model that we have derived using Lagrange equations on section 2.2.3 *Lateral/roll dynamics validity of the model around hover*. The pilot model is concatenated to the helicopter model by first expressing the transfer function of equation (62) in the time domain, which becomes,

$$-G\omega^2\theta_{1c} - 2G\zeta\omega\dot{\theta}_{1c} + k\omega^2\ddot{x} - G\ddot{\theta}_{1c} = 0 \tag{63}$$

Where the parameter *G* corresponds to kinematic ratio between the maximum cyclic blade pitch angle and cyclic lever roll angle, $\theta_{lat} = G\theta_{1c}$. Then equation (63) is added to **M**, **C** and **K** matrices, see Appendix 2, with θ_{1c} as an additional state variable. The resulting system can put into the state space form,

$$\dot{\mathbf{x}} = \mathbf{A}\mathbf{x} \tag{64}$$

With the state vector $\mathbf{x} = [\dot{\mathbf{q}}, \mathbf{q}]^T$, and the generalized coordinates vector **q**,

$$\mathbf{q} = \left[x, z, \alpha_y, \beta_0, \beta_{1c}, \beta_{1s}, \delta_0, \delta_{1c}, \delta_{1s}, \theta_{1c} \right]^T$$

The stability of the equilibrium of the bioaeroelastic system can then be assessed by computing the real part of the eigenvalues of the state space matrix **A**. As mentioned previously, literature works (Muscarello, et al., 2015) have conjectured the potential mode that can be destabilized due to pilot BDFT is the regressing lag mode as in

ground resonance phenomena[18]. The approach presented here proposes a model that proves this conjecture. Furthermore, the results show that not only the regressing lag mode can be destabilized by the pilot involuntary behavior, but also the progressive lag mode, see Figure 4-5.
A set of parameters is fixed for the helicopter and the pilot, see Table 3. These parameters correspond to a medium weight helicopter; the individual blade lag motion natural frequency ω_δ is inferior to the rotor angular velocity,

$$\omega_\delta = \sqrt{\frac{k_\delta}{I_{bl}}} = 1.53\ Hz\ \left(\approx 0.33\Omega\right)$$

The positioning of ω_δ corresponds to a soft-in-plane rotor technology ($\omega_\delta < \Omega$) and has lightly damped in-plane rotor modes, see Figure 2-22. Actually there are two very important instabilities that can develop in soft-in-plane rotor technologies with lightly damped modes which are the ground and air resonance (Krysinski & Malburet, 2011). On Figure 4-5, the real part of the eigenvalues of both regressing and advancing lag modes have been computed for varying values of potential pilot neuromuscular system settings. On those figures it is interesting to notice that the instability domains do not have the same shape and in particular that for a pilot resonant frequency above around 3Hz (~ Ω-ω_δ) the regressing lag mode recovers more and more damping even if the pilot's neuromuscular system 'stiffens'.

[18] Developed in next chapter

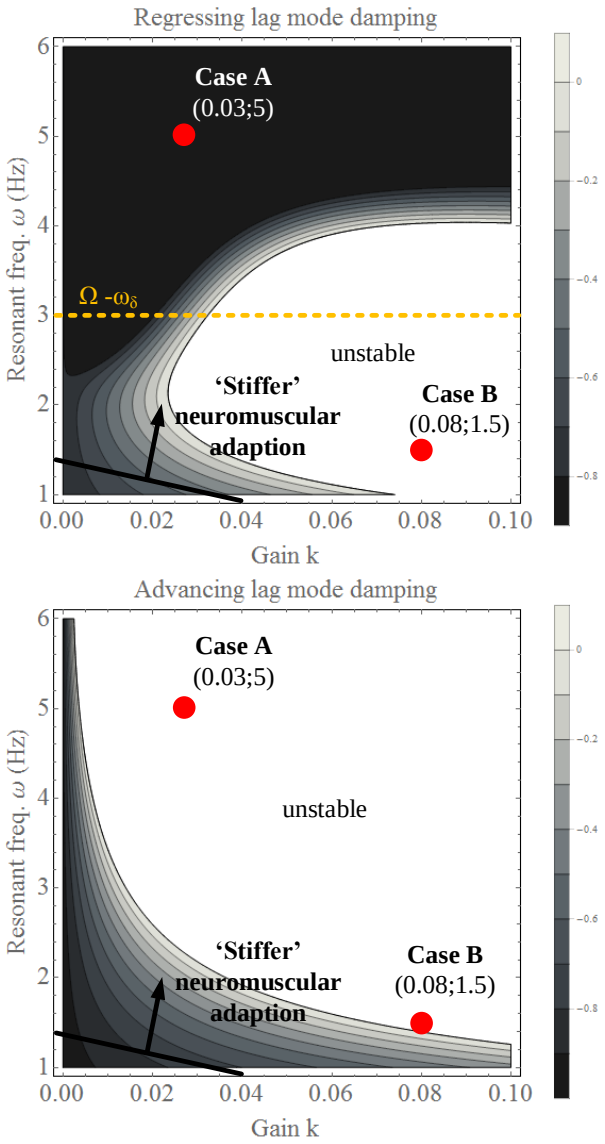

Figure 4-5. Lag modes damping for varying pilot neuromuscular system adaption

On the other side, the advancing lag mode seems to always be destabilized by any increase of pilot stiffness. In order to better understand why this might happen, the real and imaginary parts of the eigenvalues have been plotted for the case B pilot of Figure 4-5, while varying rotor angular velocities on the Campbell diagram on Figure 4-6.

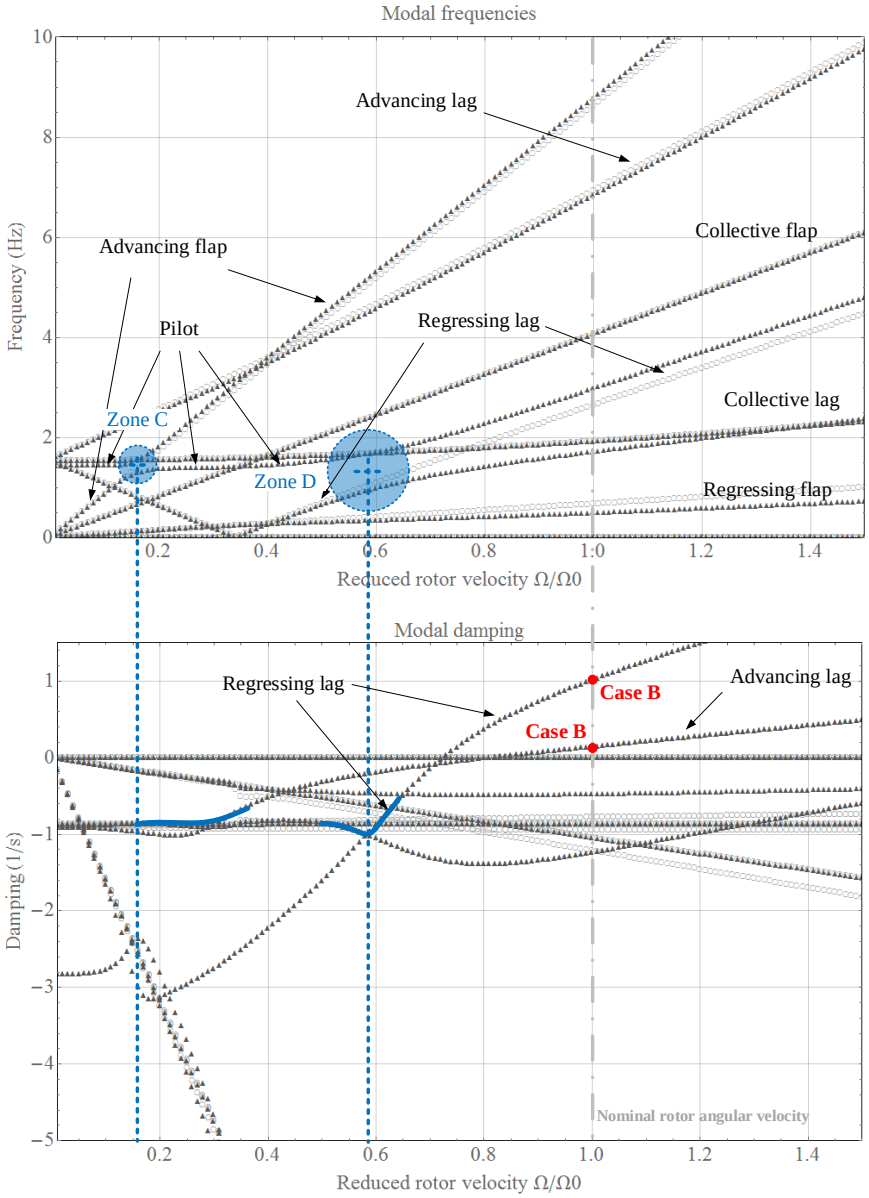

Figure 4-6. Campbell diagram, (○) no pilot biodynamics included, (▲) Case B - pilot (ω=1.5Hz, k=0.08, ζ=0.3)

The Campbell diagram of Figure 4-6 exhibits two modes that are clearly unstable when the rotor reduced velocity is higher than 1.2 which correspond to both regressing

and advancing lag modes. According to this figure, the advancing lag mode starts loosing damping at a very low reduced rotor velocity, when the pilot biodynamics mode crosses the advancing flap mode at around a reduced rotor velocity of 0.15 (Zone C). At this point, it can be conjectured that the advancing lag mode is destabilized due to the flap-lag coupling through the Coriolis effects.
On the other side, the regressing lag mode starts loosing damping when its frequency equals the pilot biodynamics mode at around a reduced rotor velocity of 0.6 (Zone D). The mechanism behind this destabilization seems to be very close to the one of ground resonance and confirms the conjecture found in literature (Muscarello, et al., 2015) "*predictions suggest that the roll/lateral PAO phenomena are more likely to occur (…) with pilots that are characterized by a natural frequency of the biodynamic poles that is close to the lightly damped in-plane rotor mode*".

4.2.2. Nonlinear time simulations

So far, the model that has been analyzed is a linear model. In this section, time simulations are performed directly from the nonlinear mathematical model obtained from the bond graph presented on Figure 4-4. Once a causal bond graph such as the one on Figure 4-4 is constructed, the most general form of mathematical model that is behind is a set of differential algebraic equations DAEs (Borutzky, 2009), with **y**(t) the state variables vector and *f* a nonlinear vector-valued function of the corresponding dimension,

$$f(\dot{\mathbf{y}}, \mathbf{y}, t) = \mathbf{0} \tag{65}$$

This equation can be obtained in a systematic manner (Borutzky, 2009) by hand or when the system becomes too large with a bond graph preprocessor such as 20-sim® software. For a reasonable DAE index[19] value, equation (65) can be numerically integrated with an adapted numerical method such as Backward Differences or Implicit Runge-Kutta, (Cuadrado, Cardenal, & Bayo, 1997), (Pennestri & Vita, 2004), (Mantegazza & Masarati, 2012). In our case a Backward Differentiation Formula (BDF) method is used, available in 20-sim®. To give an order of magnitude, there are 1600 equations to be processed by the software for the bond graph on Figure 4-4.

In order to compute the free response of the bioaeroelastic system, a perturbation is applied on the cyclic stick of the helicopter as it can be seen on the green curve of Figure 4-7. The free response on the lateral and roll axes of the helicopter in terms of velocities and rotor states using Coleman variables (beta 1s and delta 1c) are plotted. For the two pilot neuromuscular system setups, cases A and B described on Figure 4-5, the time simulation results show that the airframe oscillates respectively mainly at 7Hz and 3Hz, corresponding with the advancing and regressing lag mode frequencies, see Figure 4-8.

[19] Index: number of times the constraint equation has to be differentiated to obtain a system of ODEs (Van Dijk & Breedveld, Simulation of system models containing zero-order causal paths—I. Classification of zero-order causal paths, 1991)

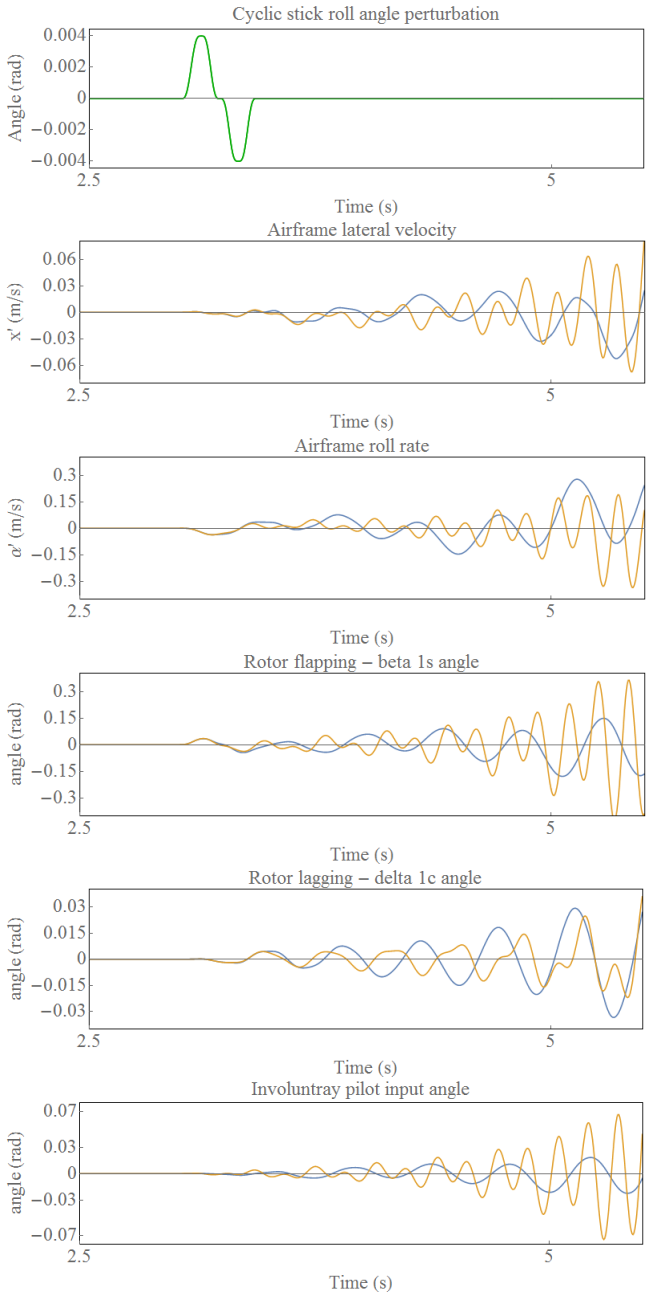

Figure 4-7. Time simulation results of the free response of the bioaeroelastic system for two pilot cases A (orange) and B (blue)

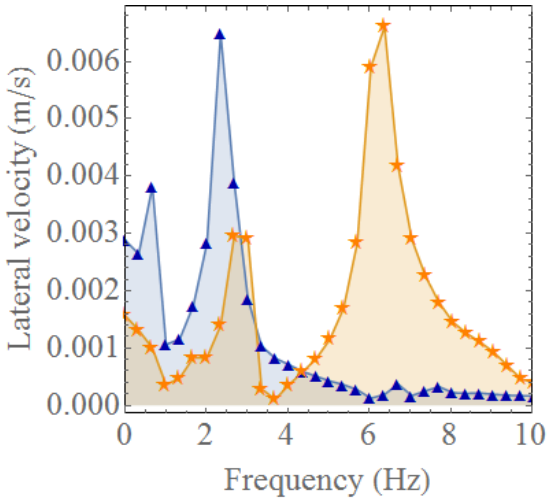

Figure 4-8. Discrete Fourier Transforms of the airframe lateral velocity free responses - case A (orange) and B (blue)

Screen captures of the 3D visualization of the simulation results have been synchronized and are presented on Appendix 5. The reader can have an appreciation of the evolution of the phenomena in a Cartesian space.

4.3. Conclusion

The first objective of this chapter, is to illustrate the *modular* or *structural approach* that is provided by the bond graph method. This was done by showing how the frontiers between subsystems of a physical system are materialized at the graphical level of a BG. This is illustrated by coupling both vehicle and pilot models developed in the previous chapters.

The human-machine model obtained represents a bioaeroelastic behavior that is then investigated more into detail; more precisely lateral-roll aeroelastic RPCs are investigated. A linear stability analysis confirms what has been conjectured in literature concerning the role played by the regressing lag mode in the phenomenon. Furthermore, the results show that for higher neuromuscular pilot stiffness's, the higher frequencies of the advancing lag mode could also excite the airframe. This last result needs to be confirmed by some experiments. It should be kept in mind that some of the assumptions taken here are reductive; especially concerning the quasi-steady aerodynamics, the flight configuration and the dry friction[20]-less cyclic lever. However, even if the predicted instability domains will move with more detailed physics, the kind of models used here will help understand the physical mechanisms behind the phenomena and could help explaining damping drops observed in real flights. Flight test results seem to be necessary here to go further.

[20] Viscous friction is taken into account

The theory of stability of equilibrium […] attracts and captivates people working in structural engineering nearly in the way ancient mythological sirens used to do with mariners, and hardly ever allows them to escape that enchanting problems.

(Perelmuter & Slivker, 2013)